

SUPPLEMENTARY INFORMATION

Intellectual Disability and Behavioral Deficits Linked to *CYFIP1* Missense Variants Disrupting Actin Polymerization

Mariano *et al.*

Supplemental Methods and Materials

Exome sequencing. Peripheral blood samples were taken from members of affected families and DNA was analyzed by comparative genomic hybridization (CGH) and whole exome sequencing (WES). Whole exome capture, next-generation sequencing, and data analysis were carried out by the Imagine Platform and Paris Descartes Platform, respectively. Libraries were prepared from genomic DNA extracted from whole blood using an optimized SureSelect Human Exome kit (Agilent) and sequenced on a HiSeq 2000 (Illumina). Sequence reads were aligned to the human genome (hg19) using Burrows-Wheeler Aligner (BWA) software. Downstream processing was carried out with the Genome Analysis Toolkit (GATK), SAMtools, and Picard Tool. Single-nucleotide variants and indels were subsequently called by the SAMtools suite utilities: mpileup, bcftools, vcfutil. All calls with a read coverage $\leq 5X$ and a Phred-scaled SNP quality of ≤ 20 were filtered out. Substitution and variation calls were made with the SAMtools pipeline (mpileup). Variants were annotated with an internal Paris Descartes bioinformatics platform pipeline based on the Ensembl database (release 67). For candidate gene identification, a *de novo* approach, an X-linked approach, and a recessive approach were applied. After exome analysis, each selected variant was confirmed by direct sequencing using BigDye dideoxy terminator chemistry and an ABI3130xl genetic DNA analyzer (Applied Biosystems) after amplification of polymerase chain reaction (PCR) using genomic DNA from patients and other family members.

Description and *in silico* analysis of sequence variants. Sequence variants in the *CYFIP1* gene are numbered starting from the first base of the ATG codon, numbered based on the reference sequence NM_014608.2. The description of the sequence (Human Genome Variation Society) was done with the assistance of Alamut Visual software (Interactive Biosoftware). The two *CYFIP1* variants were previously annotated in the dbSNP (NIH) database as: c.2225C>T is rs139576657 and c.1426A>G is rs148341871.

In silico analysis was implemented using the combined annotation-dependent depletion (CADD) tool (1) and by Alamut (Interactive Biosoftware) to predict splicing effects with SpliceSite Finder-like, NNSplice, Genesplicer, Human Splicing Finder and MaxEntScan. We also used two other splice site prediction softwares, SpliceRover, SPiCE, and SPiP (2). For *de novo* inheritance, three consecutive filters were applied to narrow down the variants to understand their contribution to the clinical phenotype of proband 1: (1) variants in proband 1 and not present in parents; (2) variants with read depth >10; and (3) rare variants in the population (Minor Allele Frequency (MAF) <1% in the 1000 Genomes Browser, ExAC database, and dbSNP137). In addition, selected variants (*De novo*, X-linked, and recessive) have been narrowed down using consecutive filters based on damage prediction scores (PolyPhen-2 (3), SIFT (4), CADD (1) and Revel (5)). SIFT scores <0.05% indicate substitutions that are predicted to be intolerant. PolyPhen-2: HumVar scores are evaluated as 0.000 (most probably benign) to 1 (most probably damaging). CADD scores >20 indicate substitutions predicted to be pathogenic. The REVEL score can range from 0 (most probably benign) to 1 (most probably damaging).

Variant validation. The variants identified in *CYFIP1* were re-tested in the nuclear family by Sanger sequencing. The specific primers for the variant regions of *CYFIP1* were designed using Primer 3 software (6). Amplified PCR products were sequenced with specific primers on an ABI3130xl genetic DNA analyzer (Applied Biosystems) using BigDye dideoxy terminator chemistry (Applied Biosystems). The primers used are the following:

CYFIP1 exon 14:

5'-TTGATGGCCTGCCGAGCGG-3':5'-CAGGTGATCGCCATGATCAA-3';

CYFIP1 exon 20:

5'-CAGCTCACCTGCACATGCCT-3': 5'-TGATAAACGGTTACGATCAG-3';

Structural modeling of the *CYFIP1* variants and *CYFIP1* protein stability. The location of the variants was modeled *in silico* on the basis of the crystal structure of the WAVE regulatory complex as previously described (7). The stability of a protein, represented by its ΔG value in kcal/mol, is a critical aspect of its structure and function. When comparing a mutant protein with its wild-type counterpart, the difference in free energy between the two is known as $\Delta\Delta G$. The introduction of amino acid substitutions can stabilize the protein ($\Delta\Delta G < 0$ kcal/mol) or destabilize it ($\Delta\Delta G > 0$ kcal/mol) by adding or removing energy. Typically, a $\Delta\Delta G$ value greater than 1 kcal/mol is considered to have a significant impact on the three-dimensional structure of the protein. To evaluate the impact of *CYFIP1* biallelic missense variants on protein stabilization or destabilization, we used FoldX 5.0 software (8) to compute the $\Delta\Delta G$ values between mutant and wild-type *CYFIP1* proteins. The FoldX 5.0 software derives its energy terms from empirical data, thereby enhancing the software's predictive power.

To model the missing loops in *CYFIP1*, we used the SWISS-MODEL web server (9, 10) and the complete amino acid sequence (UniProt Q7L576) along with the 3P8C PDB structure as a template (7). To determine the $\Delta\Delta G$ between variants and wild-type *CYFIP1*, we utilized the FoldX RepairPDB module to address residues with bad torsion angles and Van der Waals clashes. For the residues that required substitution, we utilized the BuildModel command and set the number of runs to 5. To assess the impact of missense variants, we generated Ile476Val, Pro742Leu, and biallelic substitutions.

Human fibroblast cell lines. Fibroblasts were maintained in Dulbecco's modified Eagle medium nutrient mix F-12 (DMEM/F-12) medium supplemented with 10% fetal bovine serum (FBS), 1% penicillin-Streptomycin (all Gibco, Thermo Fisher Scientific) and MycoZap Plus reagent (Lonza). Cells were cultured at 37°C in 5% CO₂.

RNA isolation and quantitative real-time PCR (RT-qPCR). Total RNA was isolated from fibroblasts or adult fly heads using TRIzol™ Reagent (Invitrogen, Thermo Fisher Scientific) according to the manufacturer's instructions. cDNA synthesis was prepared from total RNA using the Superscript III reverse transcriptase kit (Invitrogen, Thermo Fisher Scientific) and random primers (Promega Corporation). The mRNAs were quantified by quantitative real-time PCR, performed on the iCycler iQ real-time PCR detection system (BioRad) using SYBR Green-based detection (Roche) according to the manufacturer's instructions. mRNA levels of human *CYFIP1*, *NIPA magnesium transporter 1 (NIPA1)*, *NIPA magnesium transporter 2 (NIPA2)*, *tubulin gamma complex associated protein 5 (TUBGCP5)* and *ubiquitin protein ligase E3A (UBE3A)* were expressed in relative abundances compared to hypoxanthine phosphoribosyltransferase 1 (*HPRT1*) and to vinculin (*VCL*) mRNAs (11), while *Drosophila Cyfip* mRNA expression levels were normalized to the ribosomal protein L32 (*Rpl32*) mRNA, using the comparative $\Delta\Delta CT$ method. The used primers are the following:

CYFIP1 (Human):

5'-ACTTCTCCCAGGTGACCCTT-3'; 5'-CCTGCAGGACACTCTGGATG-3';

HPRT1 (Human):

5'-TGCTGAGGATTTGGAAAGGGT-3'; 5'-TCGAGCAAGACGTTTCAGTCC-3';

VCL (Human):

5'-CAGTGGATGACCGTGGAGTC-3'; 5'-CATTAGCCAGACGATGCCCT-3';

NIPA1 (Human):

5'-CAGGCTGAGCTGGAGGAAAA-3'; 5'-CGCGATCCAGAAGATGAGCA-3';

NIPA2 (Human):

5'-GACTTGCCAGGAAAGGCTCT-3'; 5'-TCACCAGCTCCCATTGACAG-3';

TUBGCP5 (Human):

5'-TCAGGTAGACAGGACACCG-3'; 5'-GCTTCGGTCATCTGGCTCAT-3';

UBE3A (Human):

5'-CAACAACCTCCTGCTCTGAGAT-3'; 5'-ACCTTCTCTTCTGTTAAGTAAGTCA-3';

Cyfip (*Drosophila*):

5'-GATCGCAATGGATTTGTCACG-3'; 5'-GGAGCACATTCAAGTTGGCAT-3';

rpL32 (Drosophila):

5'-AGCATAACAGGCCCAAGATCG-3'; 5'-TGTTGTCGATACCCTTGGGC-3'.

Western Blotting. Cells were lysed in RIPA buffer (150 mM NaCl, 50 mM Tris-HCl pH 7.4, 1% Triton X-100, 1% NaDoc, 1mM EDTA, 1:100 Proteases Inhibitor Cocktail (Sigma-Aldrich), 1:10 Phosphatases Inhibitor (Roche, Sigma-Aldrich)). Protein extracts were quantified using the Pierce™ BCA Protein Assay Kit (Thermo Fisher Scientific), separated by SDS–PAGE electrophoresis using either handmade 8% bis-acrylamide gels and SurePAGE™ 4-12% Bis-Tris (GeneScript) precast gels and transferred to a PVDF membrane (Merck, Millipore). EveryBlot blocking buffer (BioRad) was used prior to antibody incubation. The following antibodies were used: rabbit anti-CYFIP1 (21st Century Biochemicals, 1:1000)(12), rabbit anti-CYFIP1 (Millipore, Sigma-Aldrich, 1:1000), mouse anti- α tubulin (Sigma-Aldrich, 1:2000), mouse anti-Vinculin (Sigma-Aldrich, 1:2000). Membranes were then incubated with DyLight anti-mouse and anti-rabbit secondary antibodies (Invitrogen, Thermo Fisher Scientific, 1:2500) for 1 hr, (See Key Resource Table for antibodies list) and imaged with a LI-COR Odyssey scanner. Total Protein Stain (LI-COR Biosciences) was used to quantify of the total protein content. The intensity of the signal of the bands was quantified using ImageQuant (GE Healthcare), each protein of interest was normalized for α -tubulin, vinculin, and total protein content.

Surface sensing of translation (SUnSET) assay. The protein synthesis assay was performed using the SUnSET method (11). Briefly, cells were deprived of serum for 16 hours and after 4 hours of recovery in complete medium supplemented with 10% FBS, were treated with puromycin (Gibco, Thermo Fisher Scientific) 5 μ g/ml for 30 min. To validate the specificity of the assay, cells were preincubated in the absence or presence of 60 μ M cycloheximide (Sigma-Aldrich) for 15 min. After puromycin pulse, cells were chased with a fresh complete medium for 15 minutes, then washed with ice cold PBS 1X and lysed in freshly prepared RIPA

buffer. The samples were analyzed by WB and puromycin incorporation was detected using the mouse monoclonal antibody anti-Puromycin (DSHB, clone: PMY-2A4, 1:500). Total protein stain (LI-COR Biosciences) of total proteins and immunolabelling of the housekeeping protein mouse anti- α Tubulin (Invitrogen, Thermo Fisher Scientific, 1:2000), mouse anti-Vinculin (Sigma-Aldrich, 1:2000) and mouse anti-GAPDH (Invitrogen, Thermo Fisher Scientific, 1:2000), were used as the loading control.

Immunofluorescence. The cells were plated on glass coverslips and fixed with 4% paraformaldehyde (PFA) in PBS 1X for 15 minutes. After permeabilization with PBT (0.2% Triton X-100 in PBS 1X) and blocking with 10% fetal bovine serum (Gibco, Thermo Fisher Scientific), cells were incubated for 1 h at room temperature with Phalloidin-conjugated to tetramethylrhodamine (Phalloidin-TRITC) (Sigma-Aldrich, 1:1000) and DAPI (Thermo Fisher Scientific, 1:1000). Coverslips mounted with Mowiol 4-88 medium (Sigma-Aldrich) were imaged using a 63x objective (Plan Aplanachromat, NA 1.4, water immersion) in an SP8 laser scanning confocal microscope (Leica). Same confocal and laser intensity settings were used. Phalloidin-TRITC fluorescence intensity in the entire cell was quantified based on the sum of the different Z-stacks intensity projections using FIJI software (NIH). Between 50-60 cells/genotypes from different independent experiments were analyzed.

Immunoprecipitation of the CYFIP1 complex. Immunoprecipitation of the CYFIP1 protein complex followed by Western blot technique was performed using fibroblasts derived from Proband 1 and TDI. Cells were lysed using the lysis buffer containing 150 mM NaCl, 30 mM Tris-HCl (pH 8.0), 1.5% Triton X-100, 1 mM dithiothreitol (DTT), 1:10 Phosphatases Inhibitor (Roche), 1:100 Proteases Inhibitor Cocktail (Sigma-Aldrich) and 1:1000 RNaseOUT Ribonucleases Inhibitor (Invitrogen, Thermo Fisher Scientific). Lysates were centrifuged at 12000 g for 10 min at 4 ° C. Protein extracts (800-1000 μ g) were incubated with 5 μ g of CYFIP1

polyclonal rabbit antibody (Millipore, Sigma-Aldrich) or with 5 µg of anti-rabbit IgG (Santa Cruz Biotechnology) as negative control, overnight at 4 ° C. The protein-antibody complex was then incubated with 30 ml of Dynabeads™ protein G (Invitrogen, Thermo Fisher Scientific), previously saturated with 1% BSA in 1X PBS, for 3 h at 4°C. The beads were then washed three times in a buffer containing 150 mM NaCl, 30 mM Tris-HCl (pH 8.0), and 1% Triton X-100. The elution was performed by resuspending the beads in 25 µl of 4X Laemmli protein sample buffer (BioRad) and boiling the immunoprecipitated extracts at 95 ° C for 5 min. The fractions (input (20µg), IP and IgG) were separated by SDS–PAGE electrophoresis and transferred to a PVDF membrane (Merck, Millipore). EveryBlot blocking buffer (BioRad) was used prior to antibody incubation. The following antibodies were used: rabbit anti-CYFIP1 (Millipore, Sigma-Aldrich, 1:1000), rabbit anti-WAVE/Scar (Millipore, Sigma-Adrich, 1:500) and rabbit anti-NCKAP1 (Sigma-Aldrich, 1:500). The membranes were then incubated with DyLight anti-rabbit secondary antibodies (Invitrogen, Thermo Fisher Scientific, 1:2500) or anti-rabbit HRP (Cell Signaling Technology, 1:2500) for 1 h, (See Key Resource Table for antibody list) and imaged with a LI-COR Odyssey scanner or the imaging system LAS-4000 mini-imaging system (GE Healthcare) after incubation with Luminol/Enhancer Reagent (BioRad). The signal intensity of the bands was quantified using ImageQuant (GE Healthcare).

Analysis of Human CYFIP1 homologs and orthologs. The sequence of the human cytoplasmic FMR1-interacting protein 1 (CYFIP1) isoform a protein (NP_001274739.1) was aligned using Blast (NIH) against the mouse (*Mus musculus*) cytoplasmic FMR1-interacting protein 1 (Cyfip1) isoform a (NP_001158133.1), zebrafish (*Danio rerio*) cytoplasmic FMR1-interacting protein 1 homolog (NP_997924.1) and *Drosophila* specifically Rac1-associated protein 1 (Sra-1/CYFIP) (NP_650447.1). The DIOPT Ortholog Finder (<https://fgr.hms.harvard.edu/diopt-documentation>) online tool was used to assess the conservation and homology of human CYFIP1 and *Drosophila* Cyfip proteins. The DIOPT integrates human and fly ortholog predictions from the Ensembl Compara, HomoloGene,

Inparanoid, Isobase, OMA, orthoMCL, Phylome, RoundUp, and TreeFam tools, allowing the identification of orthologous genes. In addition, it returns a simple score indicating the number of tools that support the orthologous gene-pair relationship. High scores indicate that the homology between the two genes is high.

CRISPR/Cas9 generation of the *Drosophila Cyfip* knock-in mutants. The scarless genome editing approach (13) was used to generate *Drosophila* knock-in (KI) mutants carrying the *Cyfip*^{I471} and *Cyfip*^{P760L} mutations as previously described (14).

pBS-DsRed-attP-CyfipI471V wSL and *pBS-DsRed-attP-CyfipP760L wSL* cloning (Donor plasmids): the 3698 bp fragment spanning the *Cyfip* gene (CG4931) from the exon 1 to 7 was amplified by PCR using genomic DNA from nos-Cas9 (BDSC, cat. 78781) as a template, with primers (5'-gagctcgagGTCCAATGAGCAGCCGAATC-3' and 5'-gagtctagaTGACCCGCAGAATGTGGTA-3'). The amplified product was cloned into the pBS-SK vector using the XhoI and XbaI restriction enzyme sites. The resulting plasmid was used to amplify the left and right homology arms as follows.

Cloning of the Cyfip^{I471V} *allele*: the left and right homology arms were amplified by PCR with the following primers: 5'-GAGCTCGAGGTCCAATGAGCAGCCGAATC-3' and 5'-CAATATGATTATCTTTCTAGGGTAAACACCTGCAGTCCCTTTATC-3'; 5'-CGCAGACTATCTTTCTAGGGTAAATGGCGCGCATTGAAACCGTACTCTGCGAAGCTGTC CGGC-3' and 5'-GAGTCTAGATGTACCCGCAGAATGTGGTA-3'. The GTC codon sequence was introduced to induce the I > V mutation at genomic position 471 of *Drosophila Cyfip*.

Cloning of the Cyfip^{P760L} *allele*: the left and right homology arms were amplified by PCR with the following primers: 5'-GAGCTCGAGGTCCAATGAGCAGCCGAATC-3' and 5'-CAATATGATTATCTTTCTAGGGTAAAACCGAGTACCTCGCACT-3'; 5'-CGCAGACTATCTTTCTAGGGTAACTTTTCAGTCGTATCTCCGCA-3' and 5'-GAGTCTAGATGTACCCGCAGAATGTGGTA-3'. The CTC codon sequence was introduced

to induce the P > L at genomic position 760. The *3xP3-DsRed* marker cassette was amplified from the *pHD-sfGFP-ScarlessDsRed* (DGRC, cat.1365, gift from B. McCabe, EPFL, Switzerland) with primers (5'-TTAACCCCTAGAAAGATAATCATATTG-3' and 5'-TTAACCCCTAGAAAGATAGTCTGCG-3'). The generated fragments were assembled into the pBS-SK(+) vector using the NEBuilder® HiFi DNA Assembly Master Mix (New England Biolabs), following the manufacturer's instructions.

pCFD3-dU6-Cyfip gRNA(I476V) and *pCFD3-dU6-Cyfip gRNA(P760L)* cloning (gRNA plasmids): sgRNAs were designed using the online tool CRISPCan, synthesized as double stranded oligonucleotides (5'-GTCGCATTGAAACCGTATTGTGCG-3' and 5'-AAACCGCACAAATACGGTTTCAATG-3' for *I471V* mutagenesis and 5'-GTCGATTATTGCGGGGATACGAC-3' and 5'-AAACGTCGTATCCCCGCAATAAT-3' for *P759L* mutagenesis respectively), and cloned into the *pCFD3-dU6:3gRNA* vector (Addgene, cat. 49411) (15). Donor and gRNA plasmids were injected into *nos-Cas9* (BDSC, cat. 78781) embryos (*BestGene* Inc.). CRISPR homology DNA repair (HDR) transformants were screened and HDR-positive stocks were crossed with the PBac-transposase expressing line (BDSC, cat. 32070) for excision of the *3xP3-DsRed* cassette. Sanger sequencing was used to validate the correct KI of the point mutations. The final *Cyfip^{I471V}* and *Cyfip^{P760L}* mutant flies were backcrossed with the *w¹¹¹⁸*.

Filamentous (F)/ globular (G) actin Assay. F-actin and free G-actin content in fly heads was measured using the assay kit from Cytoskeleton Inc. (Cat#BK037) and following the manufacturer's instructions. Briefly, pools of 20 fly heads/sample were homogenized in F-actin lysis and stabilization buffer, incubated at 37 ° C for 10 min and centrifuged to remove the debris. The supernatant was collected and centrifuged at 100000 g at 37 ° C for 1 h to separate the G-actin from F-actin fractions. The pellet was resuspended in the F-actin depolymerization solution on ice for 1 h. F- and G- samples were quantified for the actin content by western blotting analysis using the rabbit anti-Actin (1:1000) antibody provided in the kit and anti-rabbit

800 DyLight (Thermo Fisher Scientific) as secondary antibody. The signal intensity of the bands was imaged with a LI-COR Odyssey scanner and quantified using ImageQuant (GE Healthcare) and the ratio of F-actin to G-actin for each sample was calculated.

Immunohistochemistry. The whole brain dissection of adult male flies was carried out as previously described (16). Briefly, brains were dissected on ice cold PBS 1X, fixed in 4% PFA for 20 min, and washed for 30 min with PBST (PBS 1X and 0.3% Triton-X 100). Tissues were blocked in 10% goat serum (Sigma-Aldrich) and probed with anti-Fascilin 2 (FasII) (DSHB, clone: 1D4, 1:200) and anti-PDF (DSHB, clone: 7C, 1:250). Alexa-Fluor 488 anti-mouse (Invitrogen, Thermo Fisher Scientific, cat. 1:500) was used as secondary antibody. The brains were mounted on Mowiol 4-88 mounted medium (Sigma-Aldrich) and imaged with a Leica SP8 confocal microscope using a 40x objective (Plan Apochromat, NA 1.25, water immersion). Images were taken using the same confocal and laser intensity settings.

3D morphological analysis of the axonal projections from the small lateral ventral neurons (s-LNV). Immunohistochemistry was performed between ZT2 and ZT3, to ensure maximal ramification of the s-LNVs. Dorsal branch pictures were taken using a Leica SP8 confocal microscope equipped with a 40x NA 1.25 water immersion objective. Images were acquired using the super-resolution Lightning Leica Module that performs an automatic deconvolution process. All pictures have been acquired with the same confocal settings. The maximal intensity Z projection was used for the 3D morphology analysis, using a MATLAB custom script as previously described (17). A MATLAB script was developed to automatically recreate the 3D projections of the dorsal projections of s-LNV neurons from the confocal stacks (83.10 x 83.10 μm – 1384 x 1384 pixels resolution) based on a previous publication (17). s-LNV projections starting from the point where the axons turn were selected for analysis. An additional step was taken to remove any unwanted spots prior to reconstruction. To remove

the background, a 90% threshold across the full stack of images was taken. A system of x-, y-, and z-axes was created: the x-axis (where the s-LNV axonal termini have the longest ramification) and y- axis (the orthogonal direction). The z-axis is acquired automatically from the stack, knowing that the stack moves with a 1 μm step from one image to the next. Z- layers that remained empty due to the image acquisition larger than the axon itself were removed. Finally, the images were color-coded from blue to red according to the z-axis depth.

The local spread of a 3D curve is a measure of how much the curve extends along each of its principal axes. To calculate the local spread, we first need to compute the covariance matrix of the curve. The covariance matrix is a square matrix that contains information on the variance and correlation of the curve along each of its dimensions. Once we have computed the covariance matrix, we can calculate the eigenvalues and eigenvectors of the matrix. The eigenvalues represent the variance of the curve along each of its principal axes, whereas the eigenvectors represent the direction of the corresponding axes. We then sort the eigenvalues in descending order and the eigenvectors so that they correspond to the eigenvalues. This allows us to have a measure of the local spread of the curve along the three principal axes ordered by importance, so that we can easily evaluate which axis has the greatest spread of the curve and which has the least. To quantify the local spread along each axis, we calculate the square root of the corresponding eigenvalue. This value represents the standard deviation of the curve along that axis. The standard deviation is expressed in the same unit of measure as the coordinates of the curve.

In summary, the local spread of a 3D curve is calculated by computing the covariance matrix of the axon, calculating its eigenvalues and eigenvectors, and sorting them in descending order. The local spread is then quantified by taking the square root of the eigenvalues, which represents the standard deviation along each principal axis, and it is expressed in the same unit of measure as the curve's coordinates (pixels). The 3D spread is therefore calculated by multiplying the x-, y- and z- axis spread. To calculate the volume of the axon represented as a 3D image, we counted the number of voxels (cubic elements) that belong to the axon and

multiply it by the volume of each voxel. The axonal volume provides information about morphology and growth and can be used to compute other features such as axonal density and thickness.

Mushroom body morphometric measurement. The length and the width of the α - and β -lobes of the mushroom bodies (MBs) were measured by FIJI software and expressed as values relative to the distance between the α -lobe heels, as previously (18). Values were obtained for more than 20 brains for all genotypes, thus allowing analysis of around 40 hemispheres.

Behavior assays. *Social behavior assay (competition for food).* The assay was performed on socially experienced, male flies as previously described (19, 20). Briefly, groups of eight males from the same genotype were anesthetized 24 h before the assay and placed in vials with food. On the day of the assay, males were transferred without anesthesia to an empty vial and food deprived for 90 min. Then they were exposed to a food droplet for 2 min of acclimatation. Total number of social event encounters (touching, charges, and wing rising) was video-recorded and scored for 2 min. All experiments were conducted between ZT1–ZT4 (Zeitgeber time).

Social Space behavior. Social space behavior was performed as previously described (19, 21). Male flies were collected in groups of 30 the day prior to each experiment and kept in vials with fresh food. Analysis of social space behavior was performed using a circular horizontal chamber (9 cm in diameter). Flies were placed in the chamber using cold anesthesia and allowed to acclimate for 10 min. Digital images were collected after 30 min, a time flies reached a stable position. Images were imported in FIJI and analyzed as previously (19). All experiments were conducted between ZT1–ZT4. The total distribution of the distances to the closest fly was calculated and the Kolmogorov–Smirnov test used for statistical analysis. The

social preference index was calculated as previously described (21) namely by subtracting the percentage of flies at a distance of 0.5 - 1.0 cm from the flies at 0 - 0.5 cm distance.

Rapid Iterative Negative geotaxis assay (RING). The RING assay was performed as previously reported (22). Briefly, groups of 19-20 flies were transferred without anesthesia to polystyrene vials, assembled into the RING apparatus, and allowed to acclimate for 15 mins. Carefully, the RING apparatus was sharply tapped to ensure that all the flies fell to the ground. The flies were video recorded during climbing behavior for 1 min trial followed by 1 min of rest, for a total of 5 trials. The first 3 trials were scored for analysis by 2 experimenters blind to the genotype and the percentage of flies above the 6 cm line after 9 minutes was calculated as previously described (23).

Locomotion activity assay. Locomotion assays were performed as previously (24). Briefly, fly activity was recorded for at least 3 consecutive days using the *Drosophila* Activity Monitoring (DAM) system (TriKinetics). Activity (crossing the infrared beam) was recorded over a period of 1 min and analyzed using a custom R script as previously described (14).

Supplemental Figures

Figure S1.

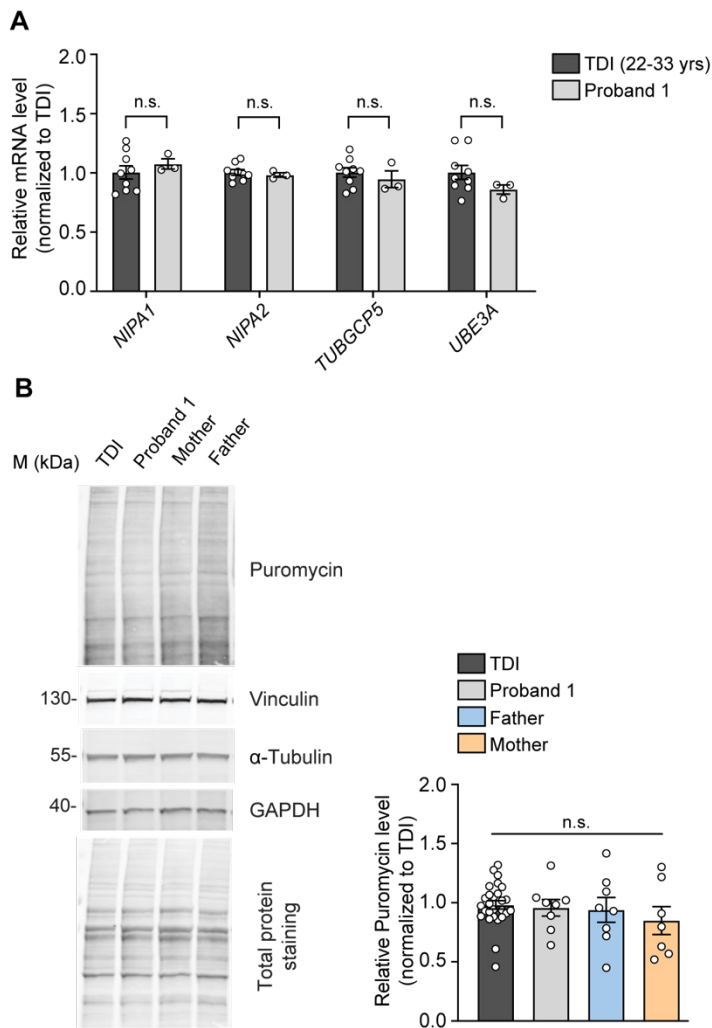


Figure S1. (A) Quantitative RT-PCR in the affected proband 1 and TDI (n = 3 lines, 22-33 years old) fibroblasts for *NIPA1*, *NIPA2*, *TUBGCP5* and *UBE3A* mRNA levels normalized to *HPRT1* and *VCL*. n = 3 independent experiments. Unpaired two-tailed Student's t-test, $p =$ n.s. not significant. Data are represented as mean \pm S.E.M. (B) Levels of global protein synthesis in human fibroblasts from proband 1, parents, and TDI (4 lines, 22-33 years old, and 3 lines 43-57 years old) fibroblasts assessed by SUnSET technique. Left, representative Western blot showing puromycin incorporation, α -tubulin, vinculin, GAPDH proteins, and total protein staining. Right, bar plots showing the quantification of puromycin incorporation normalized to vinculin, α -Tubulin, GAPDH and total protein content. TDI n = 27, Proband 1 n

= 8, Father n = 8, Mother n = 7, technical replicates, from n = 3 independent experiments.

One-Way ANOVA, n.s., not significant. Data are represented as mean \pm S.E.M.

Figure S2.

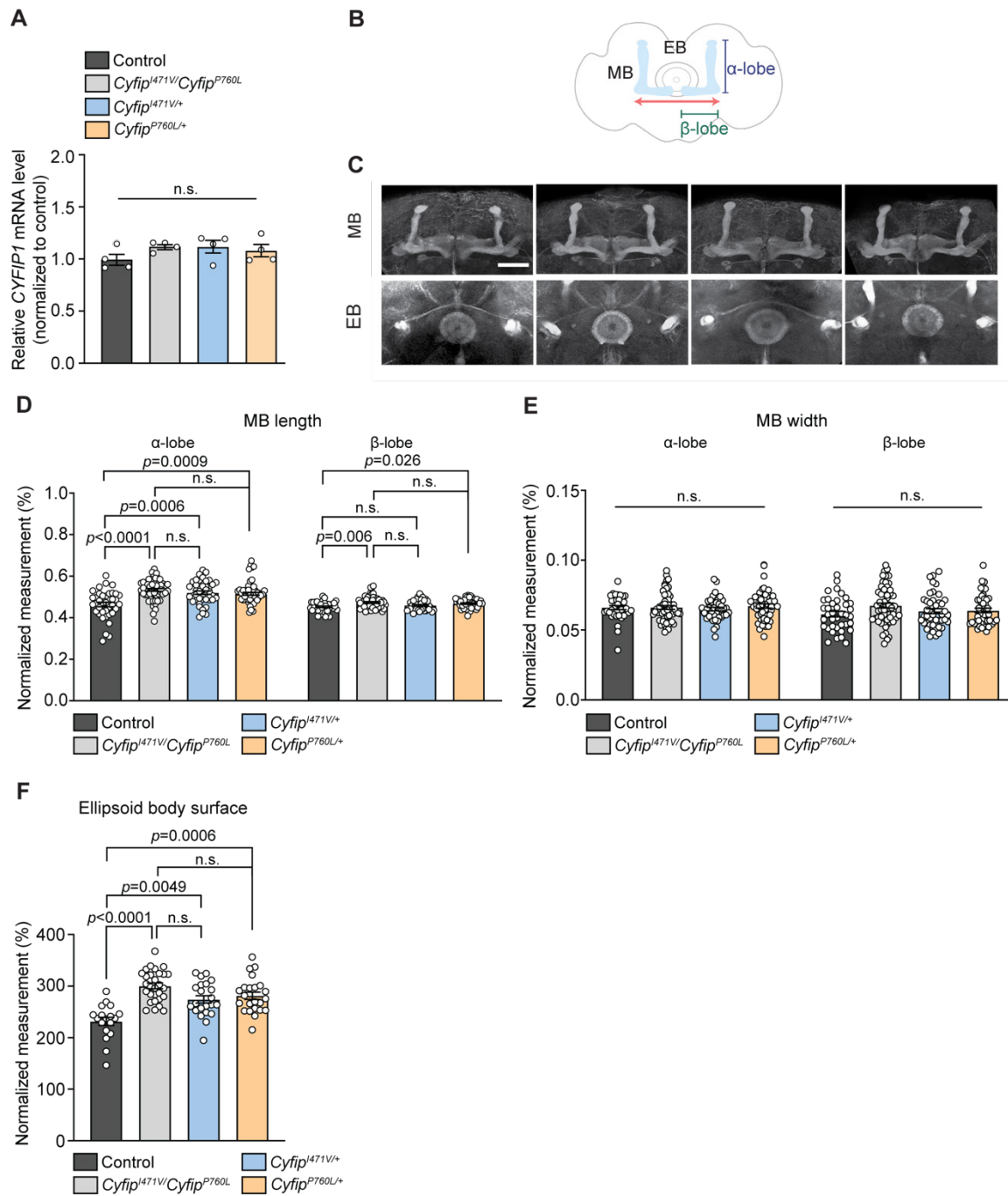


Figure S2. Molecular and morphological characterization of *Drosophila* *Cyfip* missense mutations in flies. (A) Quantification of *Cyfip* mRNA levels normalized over *rpL32*, by quantitative real-time PCR (RT-qPCR) in control and *Cyfip* KI mutant flies. $n = 4$, pool of 15 fly heads/ genotype. One-Way ANOVA, n.s. = not significant. Data are represented as mean \pm

S.E.M. (B-F) Morphometric analysis of the mushroom bodies (MB) α - and β - lobes and ellipsoid body (EB). (B) Scheme representing the anatomy of the MB and EB in the brain of an adult fly. (C) Anti-FasII staining visualizing the α -, β -lobes of the MBs and EB in the entire adult brain of 3–7-days old males of control and *Cyfi*p KI mutants (Scale bar = 50 μ m). Quantification of the length (D) and width (E) of the α - and β -lobes of the MB. n = 38 - 57 hemibrains for each genotype. Dunn's multiple comparison test following Kruskal-Wallis test, exact significant *p*-values are reported in the figure. Data are represented as mean \pm S.E.M. (F) Quantification of the EB body surface. n = 18-29 brains for each genotype. Dunn's multiple comparison test following Kruskal-Wallis test, exact significant *p*-values are reported in the figure. Data are represented as mean \pm S.E.M.

Video S1. Representative videos showing the competition for food behavior in control and *Cyfi*p^{I471V}/*Cyfi*p^{P760L} flies, related to Figure 5A.

Video S2. Representative videos of the Rapid iterative negative geotaxis (RING) behavior performed in control, *Cyfi*p^{I471V/+}; *Cyfi*p^{P760L/+} and *Cyfi*p^{I471V}/*Cyfi*p^{P760L} flies, related to Figure 5F.

Supplemental References

1. Rentzsch P, Witten D, Cooper GM, Shendure J, Kircher M (2019): CADD: predicting the deleteriousness of variants throughout the human genome. *Nucleic Acids Res.* 47:D886-D894.
2. Leman R, Parfait B, Vidaud D, Girodon E, Pacot L, Le Gac G, et al. (2022): SPiP: Splicing Prediction Pipeline, a machine learning tool for massive detection of exonic and intronic variant effects on mRNA splicing. *Hum Mutat.* 43:2308-2323.
3. Adzhubei IA, Schmidt S, Peshkin L, Ramensky VE, Gerasimova A, Bork P, et al. (2010): A method and server for predicting damaging missense mutations. *Nat Methods.* 7:248-249.
4. Ng PC, Henikoff S (2003): SIFT: Predicting amino acid changes that affect protein function. *Nucleic Acids Res.* 31:3812-3814.
5. Ioannidis NM, Rothstein JH, Pejaver V, Middha S, McDonnell SK, Baheti S, et al. (2016): REVEL: An Ensemble Method for Predicting the Pathogenicity of Rare Missense Variants. *Am J Hum Genet.* 99:877-885.
6. Untergasser A, Cutcutache I, Koressaar T, Ye J, Faircloth BC, Remm M, et al. (2012): Primer3--new capabilities and interfaces. *Nucleic Acids Res.* 40:e115.
7. Chen Z, Borek D, Padrick SB, Gomez TS, Metlagel Z, Ismail AM, et al. (2010): Structure and control of the actin regulatory WAVE complex. *Nature.* 468:533-538.
8. Schymkowitz J, Borg J, Stricher F, Nys R, Rousseau F, Serrano L (2005): The FoldX web server: an online force field. *Nucleic Acids Res.* 33:W382-388.
9. Bienert S, Waterhouse A, de Beer TA, Tauriello G, Studer G, Bordoli L, et al. (2017): The SWISS-MODEL Repository--new features and functionality. *Nucleic Acids Res.* 45:D313-D319.
10. Waterhouse A, Bertoni M, Bienert S, Studer G, Tauriello G, Gumienny R, et al. (2018): SWISS-MODEL: homology modelling of protein structures and complexes. *Nucleic Acids Res.* 46:W296-W303.
11. Jacquemont S, Pacini L, Jonch AE, Cencelli G, Rozenberg I, He Y, et al. (2018): Protein synthesis levels are increased in a subset of individuals with fragile X syndrome. *Hum Mol Genet.* 27:2039-2051.
12. Napoli I, Mercaldo V, Boyl PP, Eleuteri B, Zalfa F, De Rubeis S, et al. (2008): The fragile X syndrome protein represses activity-dependent translation through CYFIP1, a new 4E-BP. *Cell.* 134:1042-1054.
13. Gratz SJ, Ukken FP, Rubinstein CD, Thiede G, Donohue LK, Cummings AM, et al. (2014): Highly specific and efficient CRISPR/Cas9-catalyzed homology-directed repair in *Drosophila*. *Genetics.* 196:961-971.

14. Mariano V, Kanellopoulos AK, Aiello G, Lo AC, Legius E, Achsel T, et al. (2023): SREBP modulates the NADP(+)/NADPH cycle to control night sleep in *Drosophila*. *Nat Commun.* 14:763.
15. Port F, Chen HM, Lee T, Bullock SL (2014): Optimized CRISPR/Cas tools for efficient germline and somatic genome engineering in *Drosophila*. *Proc Natl Acad Sci U S A.* 111:E2967-2976.
16. Wu JS, Luo L (2006): A protocol for dissecting *Drosophila melanogaster* brains for live imaging or immunostaining. *Nat Protoc.* 1:2110-2115.
17. Petsakou A, Sapsis TP, Blau J (2015): Circadian Rhythms in Rho1 Activity Regulate Neuronal Plasticity and Network Hierarchy. *Cell.* 162:823-835.
18. Zwarts L, Vanden Broeck L, Cappuyns E, Ayroles JF, Magwire MM, Vulsteke V, et al. (2015): The genetic basis of natural variation in mushroom body size in *Drosophila melanogaster*. *Nat Commun.* 6:10115.
19. Kanellopoulos AK, Mariano V, Spinazzi M, Woo YJ, McLean C, Pech U, et al. (2020): Aralar Sequesters GABA into Hyperactive Mitochondria, Causing Social Behavior Deficits. *Cell.* 180:1178-1197 e1120.
20. Rollmann SM, Zwarts L, Edwards AC, Yamamoto A, Callaerts P, Norga K, et al. (2008): Pleiotropic effects of *Drosophila* neuralized on complex behaviors and brain structure. *Genetics.* 179:1327-1336.
21. Simon AF, Chou MT, Salazar ED, Nicholson T, Saini N, Metchev S, et al. (2012): A simple assay to study social behavior in *Drosophila*: measurement of social space within a group. *Genes Brain Behav.* 11:243-252.
22. Nichols CD, Becnel J, Pandey UB (2012): Methods to assay *Drosophila* behavior. *J Vis Exp.* [61:3795](#).
23. Madabattula ST, Strautman JC, Bysice AM, O'Sullivan JA, Androschuk A, Rosenfelt C, et al. (2015): Quantitative Analysis of Climbing Defects in a *Drosophila* Model of Neurodegenerative Disorders. *J Vis Exp.* [100:e52741](#).
24. Pfeiffenberger C, Lear BC, Keegan KP, Allada R (2010): Processing sleep data created with the *Drosophila* Activity Monitoring (DAM) System. *Cold Spring Harb Protoc.* 2010:pdb prot5520.